Koloskov, O., Jayachandran, P. T., & Yampolski, Yu. (2023). On the performance of CARISMA – Akademik Vernadsky station Schumann resonance monitoring. *Ukrainian Antarctic Journal*, *21*(1), 37–54.
https://doi.org/10.33275/1727-7485.1.2023.705

CC BY NC ND

O. Koloskov [1, 2, 3] *, P. T. Jayachandran [1], Yu. Yampolski [3]

[1] University of New Brunswick, Fredericton, New Brunswick, E3B5A3, Canada
[2] State Institution National Antarctic Scientific Center, Ministry of Education and Science of Ukraine, Kyiv, 01601, Ukraine
[3] Institute of Radio Astronomy of the National Academy of Sciences of Ukraine, Kharkiv, 61002, Ukraine

*** Corresponding author:** alex.koloskov@und.ca

On the performance of CARISMA – Akademik Vernadsky station Schumann resonance monitoring

Abstract. The main objective of this study is to evaluate the effectiveness of the CARISMA (Canadian Array for Realtime Investigations of Magnetic Activity) – Akademik Vernadsky station (65.25°S 64.25°W, Vernadsky) Extremely Low Frequency (ELF) induction magnetometer network as a planetary monitoring system for thunderstorm activity, with observation sites located in the Arctic and Antarctic regions, respectively. To achieve this, daily ELF records from Vernadsky and Fort Churchill (FCHU, 58.76°N 94.08°W) collected in January 2022 were processed and analyzed. For CARISMA, data from the FCHU site were used due to the better signal-to-noise ratio. The horizontal magnetic components of Schumann signals obtained at Vernadsky and FCHU underwent spectral and polarization processing. ELF transients were identified, and subsequent geolocation was performed as well. Both regular (quiet) thunderstorm activity periods and an unprecedented local amplification of lightning activity near the Hunga Tonga-Hunga Ha'apai volcano during its eruption on January 15, 2022, were studied. Throughout the quiet periods, ELF signal processing yielded similar characteristics of integral lightning activity derived from CARISMA and Vernadsky records, consistent with findings in the literature and previous investigations at the Vernadsky site. On the other hand, the analysis of Schumann spectra and ELF transients during the Tonga volcano eruption confirmed that most thunderstorms were concentrated within a relatively small area around the epicenter, validating the point source model for the global lightning center. This paper demonstrates that the CARISMA and Vernadsky magnetometer network is well-suited for establishing a global lightning activity monitoring and intense lightning geolocation system. Such a system can be employed to assess and study global temperature trends, monitor the growth of lightning activity in high latitudes, and detect terrestrial, atmospheric, and geospace disaster phenomena.

Keywords: Extreme Low Frequency, global climate change, lightning detection network, space weather, transient event

1 Introduction

The Schumann resonance (SR) phenomenon is a global natural electromagnetic resonance that occurs in the cavity between the surface of the Earth and the ionosphere (Schumann, 1952; Balser & Wagner, 1960). It is caused by lightning discharges creating electromagnetic waves propagating through the resonator. These waves become trapped in the cavity, making standing waves of specific frequencies known as Schumann resonances (Bliokh et al., 1980; Surkov & Hayakawa, 2014). The fundamental frequency is approximately 7.8 Hz, and the other resonant frequencies are its harmonics. The first three resonances (7.8 Hz, 14.3 Hz, and 20.8 Hz) that correspond to the Extremely Low Frequency (ELF) waveband are usually the most prominent ones (Nickolaenko & Hayakawa, 2002; 2014).

The study of global thunderstorms using SR data has become an important area of research in recent years, as it provides a way to monitor changes in global temperature (Price & Rind, 1990; Williams, 1992; Füllekrug & Fraser-Smith, 1997; Williams, 2005; Se-

kiguchi et al., 2006; Hobara et al., 2011; Williams et al., 2019; Williams et al., 2023). A significant surge (up to 300%) in lightning activity has been observed at Arctic latitudes, closely correlating with the global temperature anomaly. This temperature anomaly indicates a notable enhancement from 0.65 °C to 0.95 °C in the Arctic region between 2010 and 2020 (Holzworth et al., 2021). Nevertheless, it is important to acknowledge that there exists a degree of uncertainty associated with this finding, stemming from the time-dependent detection efficiency of the employed lightning detection network (Williams et al., 2023). Lightning activity is affected by the amount of moisture in the atmosphere, which is directly related to temperature. As the surface temperature increases, the amount of moisture in the atmosphere also increases, leading to more lightning (Price, 2000; Rycroft et al., 2000; Surkov & Hayakawa, 2014).

Lightning serves not only as an indicator and a significant driver of climate change due to its production of potent greenhouse gases (Price et al., 1997). Additionally, a strong correlation has been discovered between convective intensity and upper tropospheric water vapor, a key element influencing Earth's climate, with lightning closely associated with convective intensity (Price, 2000; Plotnik et al., 2021). The increases in lightning activity cause changes in the amplitude and frequency of the Schumann resonances, which can be detected using monitoring stations (Sentman & Fraser 1991; Sátori et al., 1996; Sátori, 1996; Nickolaenko & Hayakawa, 2002; 2014; Sátori et al., 2005; Koloskov et al., 2005; Ondraskova et al., 2009; Koloskov et al., 2020a; Peterson et al., 2021; Pizzuti et al., 2022). By monitoring SR fields, we can gain valuable insights into the impact of lightning on our planet's climate and weather patterns, contributing to a better understanding of climate change and its implications. On the other hand, the amplitude and frequency of the resonant frequencies are related to the medium properties of the Earth-ionosphere cavity (Williams et al., 2014; Bozóki et al., 2021). The size and shape of the cavity are mainly determined by the altitude and conductivity of its ionosphere boundary, that in their turn, is affected by space weather phenomena like solar flares (Sátori et al., 1996; Sátori et al., 2005), energetic particle precipitation (Schlegel & Füllekrug, 1999; Roldugin et al., 2003) etc. Thus, the Schumann resonance can be used to investigate such effects as atmospheric and ionospheric disturbances caused by solar activity (Sátori et al., 1996; Sátori et al., 2005). In addition, changes in the SR characteristics have been linked to earthquakes and other geophysical phenomena, providing a potential tool for monitoring and predicting natural disasters (Bezrodny et al., 2007; Surkov & Hayakawa, 2014; Nickolaenko et al., 2022; Mezentsev et al., 2023). The Schumann resonances also have important implications for human health, as they are thought to play a role in regulating biological rhythms and brain activity (Cherry, 2002; Price et al., 2021; Timofejeva et al., 2021; Huang et al., 2022). Overall, studying global lightning activity using SR data provides a valuable tool for monitoring global temperature changes and investigating other natural phenomena and may benefit human health.

Due to the low attenuation of lightning emission in the ELF waveband (about 0.5 dB/Mm), a few widely spaced Schumann observatories can effectively monitor lightning worldwide. The absence of industrial electromagnetic noise and local lightning activity in the polar regions makes them highly suitable for Schumann resonance measurements. That's why the Institute of Radio Astronomy (Ukraine) initiated permanent ELF observations first in Antarctica at Ukrainian Antarctic Akademik Vernadsky station (hereinafter – Vernadsky, UAS) in 2002 and later in the Arctic at Svalbard Island in 2013 (Koloskov et al., 2020a). This simple network of ELF instruments operating synchronously in different hemispheres allows observing both transient events generated by powerful lightning and Schumann resonance fields formed by the integral lightning activity. The records obtained at the Vernadsky site are among the favorites regarding the quality and length of the continuous Schumann data. Together with the Arctic ELF records (Sousy facility, Svalbard), these arrays allowed the study of daily and seasonal periodicities of SR parameters and enabled analyzing long-term interannual variations. Thus, the effect of 11-year variations of the Schumann resonance peak intensities in phase with the solar cycle was discov-

ered and interpreted (Nickolaenko et al., 2015; Koloskov et al., 2020a). The difference in the duration of the electromagnetic seasons, as observed in the southern and northern hemispheres, was determined and explained (Koloskov et al., 2022). Seasonal variations of the activity of world thunderstorm centers were calculated (Koloskov et al., 2020a). Their correlation with air temperature over land in Africa (Paznukhov et al., 2019) and South America (Paznukhov et al., 2020) was confirmed. Because of the low attenuation of ELF signals, the continuous nature of measurements, and minimal interference at the Vernadsky site, we have detected the globally most powerful lightning strikes since 2002. This database of waveforms of more than 65 billion transient events was used to analyze interannual, seasonal, and daily variations of intense lightnings associated with transients (Koloskov et al., 2020b; Shvets et al., 2022). The concurrent ELF records available from the Sousy site in the Arctic allow for calculating positions of intense lightning strokes. However, due to the high amplitude of the 50 Hz power line harmonic at Sousy, the Arctic waveforms must be filtered with a bandpass filter of 3–30 Hz, reducing the geolocation accuracy. In addition, the Sousy facility operates in a fully autonomous mode and is difficult to visit, so malfunctions, if any, can lead to long-term data loss. Therefore, an alternative site in the Arctic is desirable.

The paper discusses the advantages, prospects, and performance of the SR observation network based on the ELF data of the CARISMA (Canadian Array for Realtime Investigations of Magnetic Activity) (Mann et al., 2008) and the Vernadsky sites located in the Canadian Arctic and the Antarctic, respectively. New ELF data arrays recorded at Fort Churchill (FCHU) CARISMA site (58.76°N 94.08°W) and Vernadsky (65.25°S 64.25°W) during January 2022 were processed and analyzed. This study uses FCHU records because they demonstrate the best signal-to-noise ratio compared to other CARISMA sites. These datasets reflect the regular behavior of the SR field and the huge local amplification of lightning activity in the vicinity of the Hunga Tonga-Hunga Ha'apai volcano during the eruption on January 15, 2022. Both variations of Schumann resonance parameters and the increase in ELF transient events during the eruption are presented and analyzed. We applied the data processing techniques outlined in (Koloskov et al., 2005; 2013; 2020a; 2020b; 2022; Shvets et al., 2022) to handle the SR field and ELF transient data. These algorithms were thoroughly validated by comparing the processing results from Vernadsky and Sousy with those obtained from various ELF observation sites situated in low, mid, and high latitudes (Sátori et al., 2016; Bozóki et al., 2021; Bozóki et al., 2023) using alternative computational methods. The advancement of the data processing methodology, while crucial, falls outside the scope of this study and is earmarked for future research efforts.

2 Data and methods

2.1 Ukrainian ELF sites

This paper discusses the results of monitoring and processing Schumann resonance signals recorded since March 2002 at the Vernadsky in West Antarctica. Similar observations were started in October 2013 at the Sousy site (78.17° N 15.99° E) on Svalbard Island, part of the Tromsø Geophysical Observatory of the Arctic University of Norway. The signals at both observation sites are recorded using identical induction-coil magnetometers (LEMI-112E) manufactured by the Lviv Center of the Institute for Space Research (Ukraine). Two orthogonal horizontal magnetic field components are recorded along South-North (SN) and West-East (WE) geographic cardinal directions. The frequency band ranges from 0.001 to 80 Hz, and the manufacturer calibrates both types of sensors to record ELF fields in absolute units. The signal waveforms are continuously recorded in digital form by 24-bit ADCs with sampling frequencies of 320 Hz at UAS and 256 Hz at Sousy, respectively. The data are synchronized using GPS timestamps. UAS is the primary Ukrainian SR observatory and provides the most extended uninterrupted data series, with only one long data gap from September 2009 to March 2010 due to a measuring system failure. The UAS dataset has better quality than Sousy's records, mainly due to the comparatively low amplitude of power harmonics (50 Hz and higher), which allows the com-

pensation method (Shvets et al., 2003) to be used at UAS to reduce 50 Hz interference. In contrast, traditional analogue and digital notch filters introduce additional biases in the pulsed waveforms. Therefore, we will discuss the data obtained at the UAS site further in the paper.

2.2 CARISMA sites

CARISMA (https://www.asc-csa.gc.ca/eng/sciences/geospace-observatory-canada-initiative.asp) is a component of the Geospace Observatory Canada project (The Geospace Observatory). CARISMA array covers the range of longitude from Rankin Inlet, NU (267.89°E) to Dawson City, YK (not far from Alaska, 220.89°E) and a range of latitudes from Osakis, MN, USA (45.87°N) to Taloyoak, NU (69.54°N). It consists of 28 sites (see Mann et al., 2008). Most of these sites are placed on a North-South meridian called the "Churchill Line". The CARISMA network incorporates fluxgate and induction coil magnetometers, but we will discuss only the latter (8 sites). Typical phenomena that can be observed using these devices include the Schumann resonances, the evidence of the ionospheric Alfvén resonator (Surkov & Hayakawa, 2014), and the signature of electromagnetic ion cyclotron waves (EMIC) in the magnetosphere (Gurnett & Bhattacharjee, 2017). The induction coils used in the CARISMA array are LEMI-30 sensors manufactured by the Lviv Centre of Institute for Space Research; they are designed for measurements in the waveband of 0.001 Hz to 30 Hz. Two coils are located at each site, aligned orthogonally with magnetic North and East. The magnetometers operate at 100 samples per second by a 24-bit acquisition system equipped with a GPS receiver for timing. For most CARISMA sites, data from the induction coil magnetometers are available from 2014 until now and can be downloaded in CDF and ASCII formats. In this study, we have opted to utilize records from the FCHU site as they exhibit the most favorable signal-to-noise ratio compared to other CARISMA sites.

2.3 Methodology

We used the algorithms described in (Koloskov et al., 2005; 2013; 2020a; 2022; Shvets et al., 2022) for SR data processing. These algorithms include finding the spectral and polarization parameters of the first three Schumann resonance modes. To compute the spectral parameters, the daily records of the field components $H_{NS} = H_x$ and $H_{WE} = H_y$ are divided into 144 intervals of 10-min duration. For each interval, we calculated the power spectra S_{xx}, S_{yy}, and cross-spectrum S_{xy} of horizontal field components with a frequency resolution of 0.1 Hz.

$$S_{ik}(f) = \frac{1}{N}\sum_{p=1}^{N} \tilde{H}_i^{(p)}(f)\tilde{H}_k^{(p)*}(f), \tag{1}$$

$$\tilde{H}_{i,k}^{(p)}(f) = \frac{1}{T}\int_{(p-1)T}^{pT} dt H_{i,k}(t) e^{-i2\pi ft} \tag{2}$$

($i, k = x, y$, $p = 1, 2, 3$ – the number of SR modes). The power spectra are used to determine the intensities and peak frequencies $f_{xx,yy}^{(p)}$ (where: f_{0p} – regular mean frequency of SR mode p; Δf_p regular mean half width of SR peak for mode p; $\Delta f_p \equiv 1.5$ Hz) computed using the following equation relevant to the method of moments:

$$f_{xx,yy}^{(p)} = \frac{\int_{f_{0p}-\Delta f_p}^{f_{0p}+\Delta f_p} f \cdot S_{xx,yy}^{p}(f)df}{\int_{f_{0p}-\Delta f_p}^{f_{0p}+\Delta f_p} S_{xx,yy}^{p}(f)df} \tag{3}$$

It's worth noting that equation (3) determines peak frequency as a continuous value. Thus, we estimate peak frequency with a resolution better than 0.1 Hz.

To derive the polarization characteristics, we calculate the Stokes parameters: I, Q, U, V (Born & Wolf, 1959):

$$I(f) \equiv S_{xx}(f) + S_{yy}(f),\ Q(f) \equiv S_{xx}(f) - S_{yy}(f),$$
$$U(f) \equiv 2\,\mathrm{Re}\,S_{xy}(f),\ V(f) \equiv 2\,\mathrm{Im}\,S_{xy}(f). \tag{4}$$

Then, using the known relations (Born & Wolf, 1959), the polarization parameters of the field are derived:

$$r = \frac{V}{\sqrt{Q^2+U^2} + \sqrt{Q^2+U^2+V^2}}, \tag{5}$$

$$\left.\begin{matrix}\sin(2\Psi)\\ \cos(2\Psi)\end{matrix}\right\} = \frac{1}{\sqrt{Q^2+U^2}}\left\{\begin{matrix}U\\ Q\end{matrix}\right., \quad (6)$$

$$I_p = \sqrt{Q^2+U^2+V^2}, \quad (7)$$

$$P = I_p / I. \quad (8)$$

Where r is the coefficient of ellipticity, 0 corresponds to the linear polarization, and 1 corresponds to circular polarization. Ψ is the position angle of the polarization ellipse, which is the orientation of the major semi-axis of the ellipse counted clockwise from the direction to the north. I_p is the intensity of the polarized radiation component. P is the degree of polarization. By studying changes in the polarization parameters, we can conclude the dynamics of the SR excitation sources. For example, the normal to the position angle indicates the direction of the source. At the same time, the total intensity and intensity of the polarized component characterize the levels of global thunderstorm activity. Our analysis uses daily arrays of spectral and polarization parameters and daily arrays averaged for month intervals. We calculated these parameters for the first three Schumann peaks. However, in this study, we analyze only the fundamental mode (first SR peak) as it is the most intense and the easiest to interpret. Analyzing the

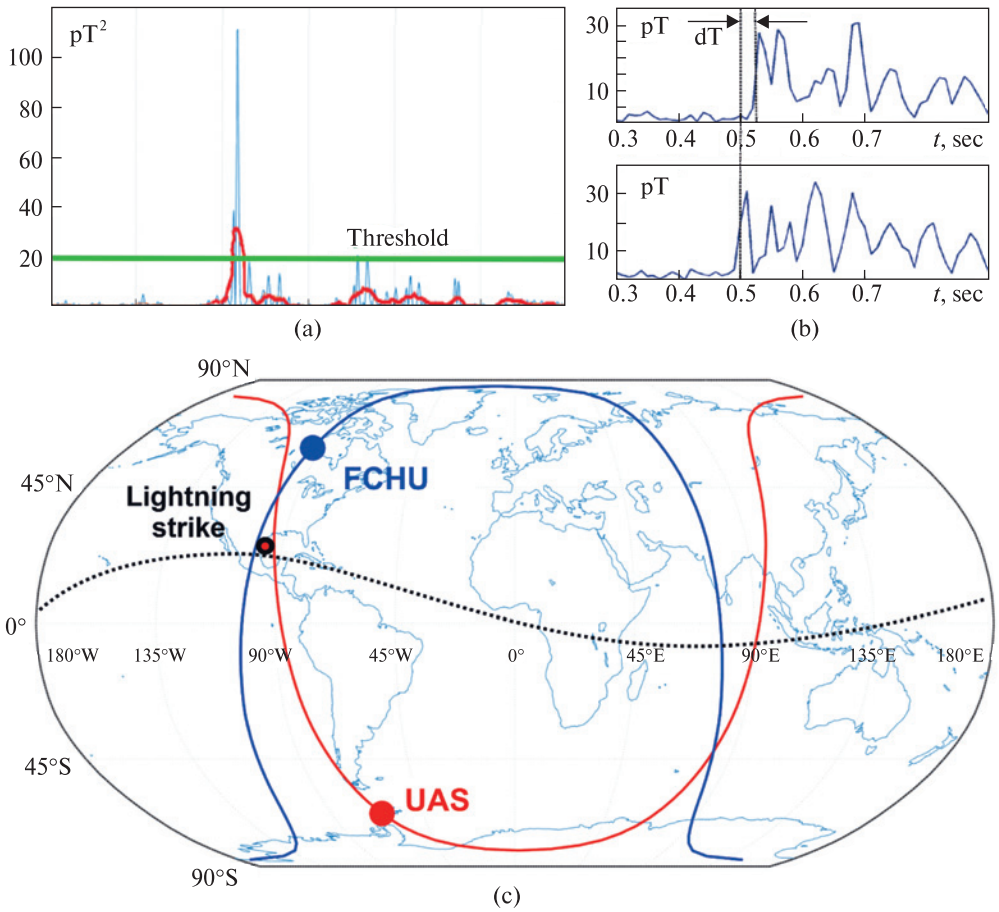

Figure 1. Scheme demonstrating the lightning geolocation technique. (a) Finding the transients exceeding the threshold level, (b) calculating the difference of the times of arrival to UAS and FCHU and calculating the distance line – black dashed line on panel c, (c) worldmap with great circles corresponding to the azimuths to the source calculated at UAS (red) and FCHU (blue) sites and distance line – black dashed line. The probable location of the source corresponds to the center of the circle (shown in red with a black outline) inscribed into the smaller triangle produced by the azimuth and distance lines

higher SR modes is beyond the scope of the current study and will be addressed in future research.

In addition to the SR noise-like signals, we observe waveforms produced by powerful lightning discharges, known as Q-bursts (transient events). With the selected threshold equal to 2.5 median values of the standard deviation of the ELF field, we typically detect one transient every 8–10 seconds. The bursts synchronously detected at the Antarctic and Arctic sites (Fig. 1a) are used to geolocate signal sources. Figure 1 explains the geolocation technique. We find the azimuth to the source at each observation point (shown by red and blue great circles in Fig. 1c) by rotating the coordinate system so that the recorded orthogonal magnetic components H_x and H_y of the transient's waveform turn into the longitudinal component H_ρ (with minimal amplitude) and the transverse component H_t (with maximal amplitude). Then, we calculate the difference in the distance line (black line in Fig. 1c) by estimating the difference in times of arrival (Fig. 1b) from the cross-correlation function of the transverse components of a transient. Following (Füllekrug & Constable, 2000), we assume that the most probable location of the source is the center of the circle inscribed into the smaller triangle produced by the azimuth and distance lines, while the area of the circle corresponds to the geolocation uncertainty. As was mentioned above, the ELF data at UAS were corrected by compensation of 50 Hz peak and their harmonics. This allows us to expand the effective frequency range to approximately 70 Hz. The data at Fort Churchill needs to be corrected because the local amplitude of the 60 Hz line is quite small, and it is effectively removed by band pass filters embedded into LEMI-30 sensors.

3 Results

In this section, we perform a comparative analysis of the data obtained at UAS and FCHU during January 2022. This interval was selected for two reasons. Firstly, January corresponds to the middle of winter in the Northern Hemisphere, when the global thunderstorm centers are located southernmost. This means there are minimum local thunderstorms at the FCHU site, which provides maximal signal-to-noise values for the Arctic observation point. The UAS has no local lightning throughout the year because the Drake Passage separates it from the South American continent. Secondly, on January 15, 2022, the most substantial local amplification of lightning activity was initiated by the Hunga Tonga-Hunga Ha'apai volcano eruption. During the eruption peak, the number of lightnings in a 300 km radius of the volcano exceeded the number of lightnings occurring in all other areas of the Earth. This event provides a unique opportunity to test the adequacy of the simplest point model of the center of global thunderstorm activity, which is often used in interpreting experimental observations. Table 1 depicts the geographic and geodetic coordinates of both sites. It is worth noting that due to the displacement of the geographic and geomagnetic poles, the UAS site has a polar geographic location and mid-latitude geomagnetic location (L-shell is 2.1). In contrast, FCHU is sub-polar geographically and polar geomagnetically (L-shell is 7.4).

3.1 Global thunderstorm activity derived from Vernadsky and CARISMA ELF records

Characteristics of global thunderstorm activity were derived from monthly averaged diurnal variations of SR signal parameters calculated at UAS and FCHU sites. It is worth noting that when calculating the average values of the Schumann fields, January 15 was excluded from the averaging to avoid distorting the average monthly characteristics of world thunderstorms. Figures 2a and b show the average daily vari-

Table 1. Geographic (CGM) and geodetic coordinates of Fort Churchill and Vernadsky stations

Station	Site Code	Geodetic Latitude	Geodetic Longitude	CGM Latitude	CGM Longitude	L-shell
Fort Churchill	FCHU	58.763 N	265.920 (94.08 W)	68.32	333.54	7.4
Vernadsky	UAS	65.231 S	295.745 (64.255 W)	–51.40	9.14	2.1

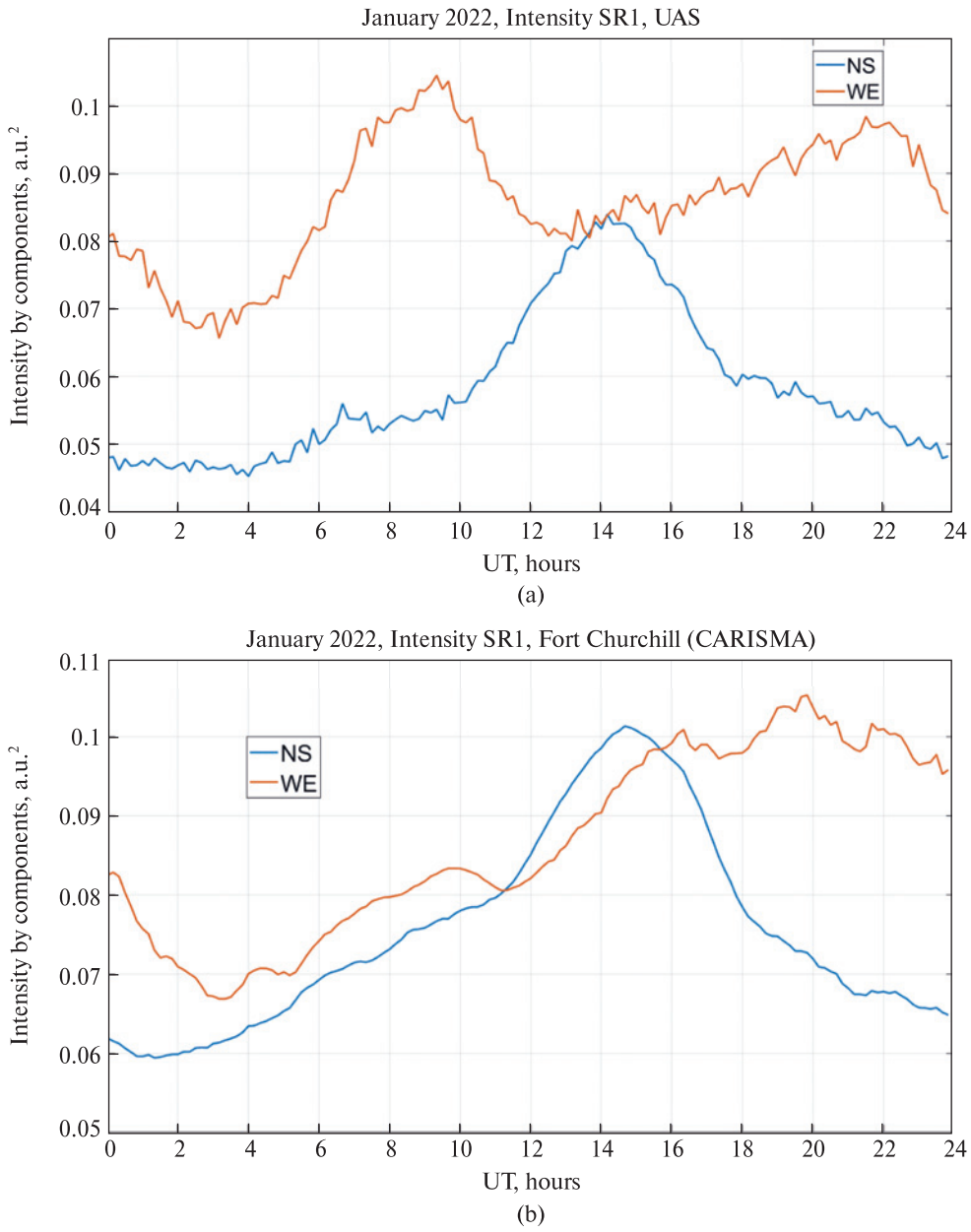

Figure 2. Averaged over the month intensity by components (NS – Africa, WE – America, Asia) of SR1 measured at (a) UAS and (b) Fort Churchill sites

ations of the North-South and West-East components of the horizontal intensity of magnetic fields for the first SR mode (SR1) at the UAS and FCHU sites, respectively.

It should be noted that the NS sensors' orientation at both sites makes them more sensitive to the thunderstorms occurring in Africa the WE sensors correspond to the lightning strokes above Asia and America. In agreement with the literature data on the culmination of world thunderstorm centers (Bliokh et al., 1980; Nickolaenko & Hayakawa, 2002; 2014), the intensity of the North-South components at both

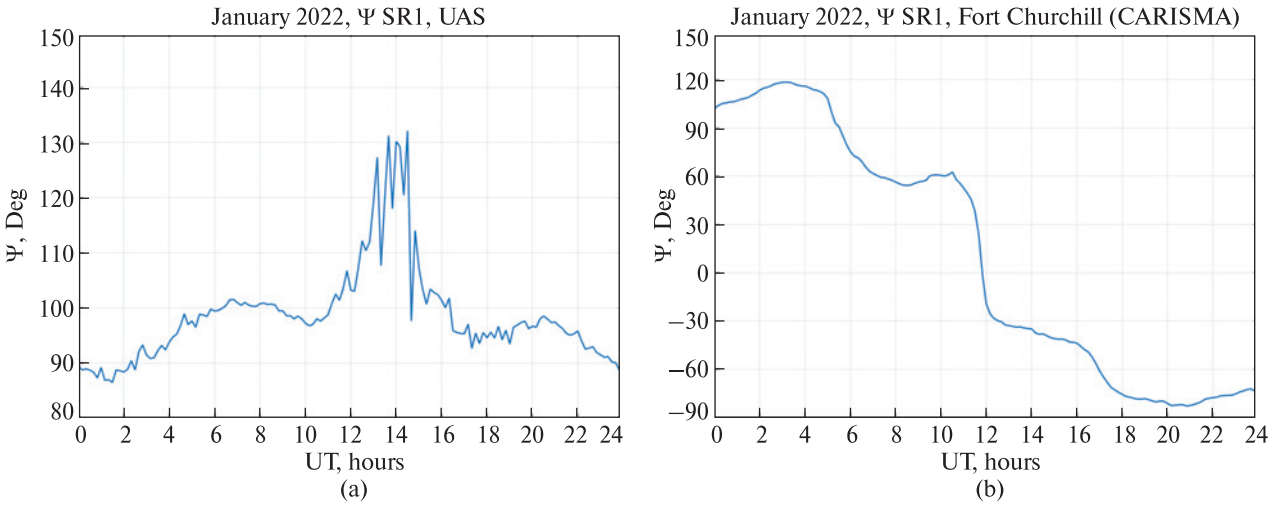

Figure 3. Mean position angle (ψ, in Deg) of SR1 polarization calculated at (a) UAS and (b) Fort Churchill sites

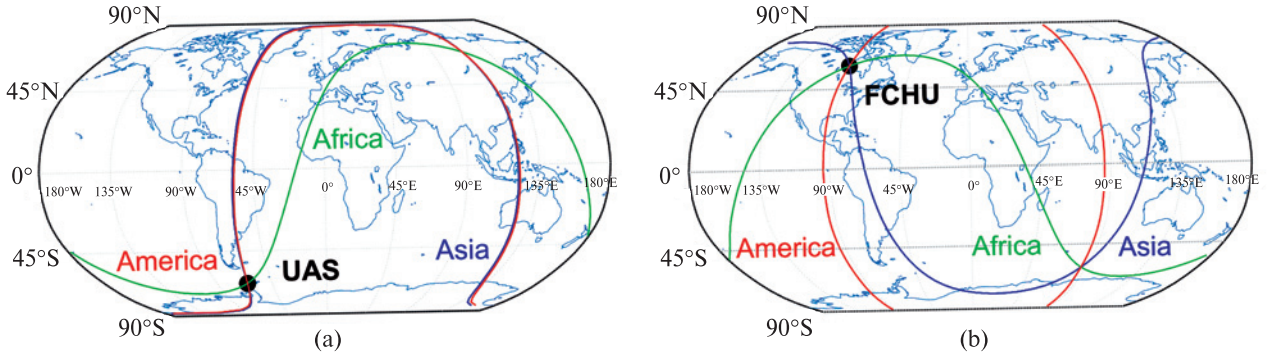

Figure 4. Azimuths (bearing lines) derived from the position angle of SR1 to Asian (in blue), African (in green), and American (in red) thunderstorm centers, respectively, at (a) UAS and (b) Fort Churchill (FCHU) sites

sites demonstrates one maximum, corresponding to approximately 15 UT, and two peaks are observed in the West-East component at about 9 UT and 21 UT. UAS data show a similar increase in the peak intensity relative to the noise level for all centers. For the FCHU peak, the intensity corresponding to the Asian thunderstorm center is less than that of the African and American. This may be due to the seasonal drift. In January, thunderstorm centers approach the UAS and move away from the FCHU as far as possible. At the same time, the Asian center is the most distant one from Fort Churchill.

Figures 3a and b depict the monthly averaged diurnal variation of the position angle calculated for the Vernadsky and Fort Churchill sites. This parameter can be used to estimate the azimuths to the world thunderstorm centers at each observation point that are orthogonal to the position angle during the culmination of each center. One can see that the variation of the position angle at UAS has one peak corresponding to the African center. At the same time, Ψ at FCHU demonstrates its steps at the culmination of each center. The different shapes of the curves may be explained by the ambiguity in 180 degrees when calculating the position angle.

Figures 4a and b show great circles constructed for directions orthogonal to the position angles at the time of the culmination of world thunderstorms. For

both observation points, the circles are aligned with the azimuths of the thunderstorm centers. Minor deviations occur for the African Center in its direction determined from the UAS (green curve in Fig. 4a) and for the American Center in azimuth estimation from the FCHU (red curve in Fig. 4b).

3.2 Lightning amplification during Hunga-Tonga volcano eruption on 2022

The Hunga Tonga event on January 15, 2022, was the largest volcanic eruption ever accurately recorded by modern instrumentation (Astafyeva et al., 2022). The

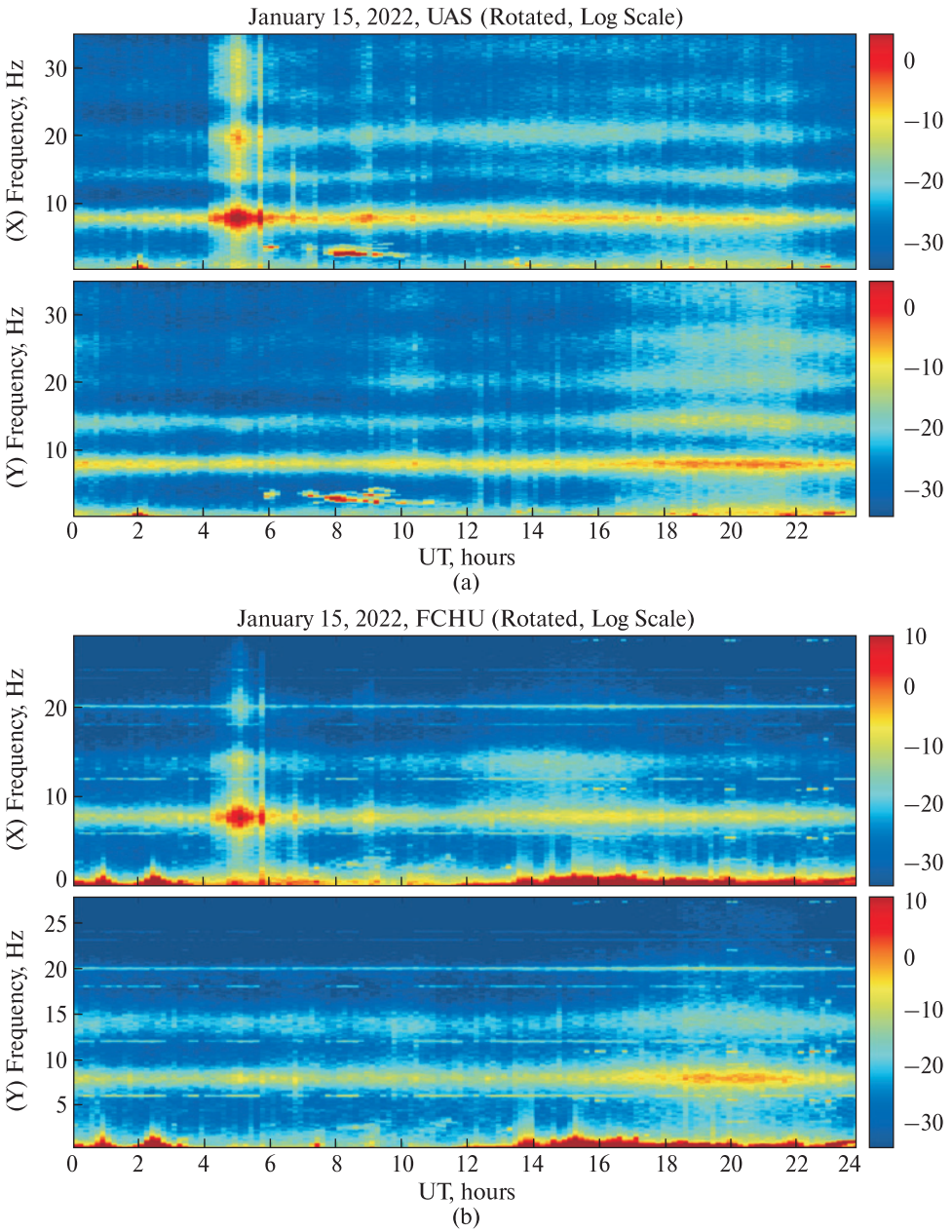

Figure 5. Spectrograms for January 15, 2022. Upper panels correspond to the intensity rotated to the azimuth of Tonga volcano: (a) UAS and (b) FCHU sites

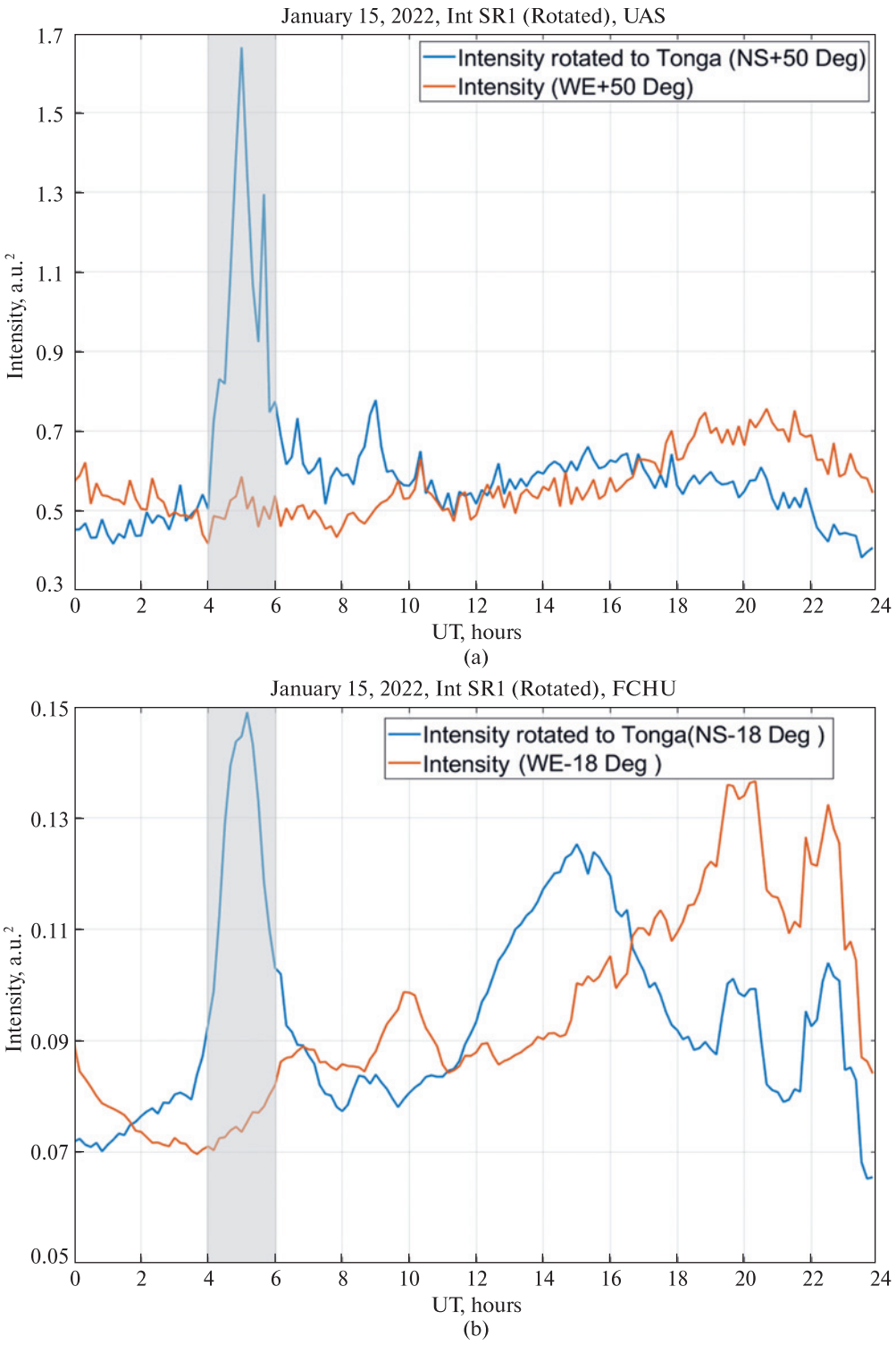

Figure 6. Intensities of the SR1 components for January 15, 2022. Gray areas indicate the main phase of the eruption. Blue lines correspond to the intensity rotated to the azimuth of Tonga volcano: a) UAS and (b) FCHU sites

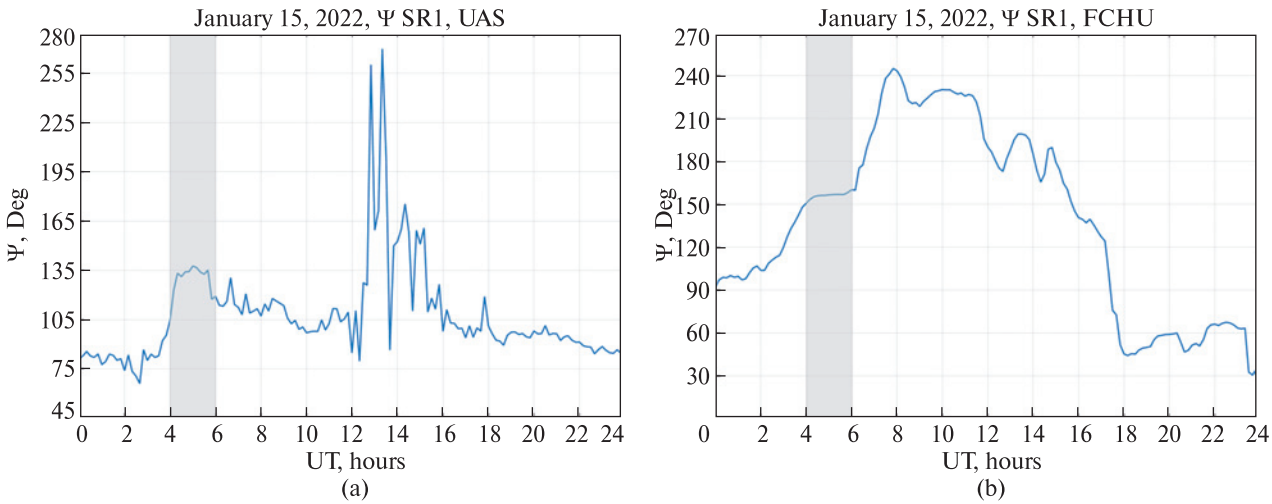

Figure 7. Position angles of the SR1 components for January 15, 2022. Gray areas indicate the main phase of the eruption: a) UAS and (b) FCHU sites

volcanic eruption has various global consequences, both short-term and long-term, affecting the ionosphere, atmosphere, ocean, and lithosphere. Several studies have demonstrated an unprecedented increase in lightning activity during the eruption. According to the ground-based global lightning detection network GLD360, owned and operated by Vaisala, almost 400,000 strikes were recorded in 6 hours, and about half occurred between 5 and 6 UT. At 5 UT, GLD360 recorded a peak of 25.508 strikes in 5 minutes (Vagasky & Said, 2022). It is worth mentioning that long-term observations of lightning flashes from space (Christian et al., 2003) estimate that the average number of lightning strikes on Earth is as high as 50 per second. It is easy to estimate that during the peak phase of the eruption, the number of lightning strokes in the vicinity of Tonga corresponded to 170% of the total flashes occurring on average on Earth. Another unique characteristic of the Tonga event is the compact size of the area of intense lightning associated with the eruption. Mezentsev et al. (2023) showed that all eruption-associated discharges were confined mainly within a circle of a 200 km radius, with some extension at the southwest up to 300 km. Thus, the Tonga event is a unique opportunity to test the point source model frequently used to diagnose global thunderstorm activity.

Our observations conducted in Antarctica and the Arctic have shown that the local amplification of lightning activity in the vicinity of Tonga has enormously intensified SR ELF fields all around the planet. Figure 5 demonstrates the increase in the intensity of all detectable modes of the SR signal at UAS and FCHU. The magnetic field components are depicted in a coordinate system rotated so that the x-axes (shown in the top panels for each site) correspond to "tangential" field components that are orthogonal to the source direction. Since the polarization of the magnetic field of a point source is close to linear, the tangential components demonstrate the maximum response to the event. In contrast, the "normal" components (corresponding to the y-axes, shown in the lower panels) practically do not react to an eruption. This behaviour of the components is well-observed both in the spectrograms and in the intensity variations of the components for the fundamental SR mode, as shown in Figure 6.

The rotation angles of the coordinate systems at each observation point were determined from the average value of the position angles during the maximum phase of the eruption (see Fig. 7). It should be noted that differences in the daily variations of the position angle (Fig. 7) outside the maximum phase of the eruption from similar average monthly variations

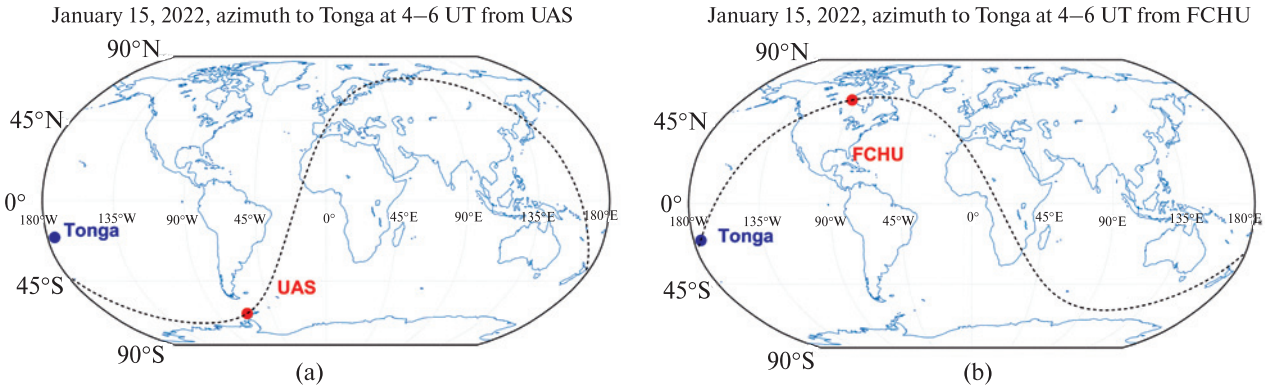

Figure 8. Azimuths (bearing lines) derived from the position angle of SR1 (4–6 UT) at a) UAS and (b) FCHU sites

(Fig. 3) are associated with the ambiguity in determining the position angle (in π value). The corresponding azimuths to the source (as shown in Fig. 8) are consistent with the calculated directions to the epicenter of the eruption. The performed analysis confirms the validity of the point model of the source and demonstrates the feasibility of using spectral and polarization analysis to determine its characteristics.

We also analyzed the ELF transients corresponding to intense lightning strikes during the Tonga eruption and used geolocation techniques to calculate the spatial distribution of the sources. The Vernadsky data set served as the reference. First, we selected ELF transients for Vernadsky and conducted geolocation for the transients with their counterparts Fort Churchill. The transients were selected based on the value of the ratio R of the standard deviations of the tangential ($STDdef_x$) and normal ($STDdef_y$) components.

$$R = STDdef_x / STDdef_y. \quad (9)$$

We used the following threshold values for R (R_{thr} = 1.5, 2, 2.5, 3, 3.5). A burst was selected when R exceeded the corresponding value for R_{thr} at all observation points. Table 2 depicts the number of chosen transients for different R_{thr} values.

Table 2. Number of transients (N) via the R_{thr} value for January 15, 2022 (04:00–06:00 UT)

R_{thr}	1.5	2.0	2.5	3.0	3.5
N	3743	2460	1057	247	40

Figure 9 presents distribution of intense lightning as observed from UAS-FCHU for R>2.5 during 04:00–06:00 UT.

The area of intense lightning discharges shown in Figure 9 has a relatively compact size that agrees well with the data of independent lightning location networks (Vagasky & Said, 2022; Mezentsev et al., 2023). Thus, from a geophysical point of view, the geolocation of ELF transients confirms the significant local increase in intense lightning associated with the Tonga eruption. During the main phase of the event, a new compact center of intense lightning emerged. As no regular center culminates from 4 to 6 UT, the number of intense lightning in the eruption-associated center within 4–6 UT exceeded the number of powerful lightning from all other areas by several orders of magnitude.

4 Discussion

An analysis of the monthly SR records for January 2022, obtained in the Antarctic Peninsula region (UAS) and the Canadian Arctic (CARISMA array), demonstrated this two-position network's excellent data quality and high efficiency for monitoring global thunderstorm activity. It has been shown that spectral and polarization processing of the horizontal magnetic components of Schumann signals obtained at UAS and CARISMA, and the selection of ELF transients with subsequent geolocation (using algorithms previously verified at Vernadsky), allows for

monitoring the integral world thunderstorm activity and intense lightning discharges. The validity of these techniques and software (previously used at UAS) has been tested by analyzing the monthly dataset of background Schumann signals and interpreting the data from the most significant increase in lightning activity recorded during the eruption of the Tonga volcano. During this event, a global lightning center formed in the vicinity of the epicentre and could be considered a point source.

It should also be noted that during the powerful Tonga event, the detection efficiency of the described ELF system remained constant, while it was significantly reduced for other lightning detection networks like WWLNN and GLD360 (Vagasky & Said 2022; Bór et al., 2023; Mezentsev et al., 2023). Thus, the ELF network may be helpful for monitoring natural hazards like the Tonga eruption. The advantages of the ELF lightning diagnostics system based on UAS and CARISMA are as follows:

• The minimum level of technogenic and natural interference at observation points guarantees stable high quality of the data. This, and the continuous nature of observations, allow for tracking all significant geo-heliophysical events occurring on the planet and in the near-earth environment.

• Using subpolar observation points in the two hemispheres ensures almost the same efficiency in diagnosing integral and super-powerful thunderstorm activity throughout the planet. With the existing geometry of the receiving points, the maximum accuracy of calculations is achieved over the American continent, where a large number of systems for diagnosing lightning activity and atmospheric and space weather are located. This simplifies the validation of ELF data and the comparison of lightning activity with the state of the near-earth environment.

• Continuous observations have been carried out since 2002 at Vernadsky and since 2014 by CARISMA. The presence of long series of observations, identical equipment (sensors manufactured by the Lviv Center of Institute for Space Research are used at both sites), and observation techniques guarantee the detection efficiency's invariance during the entire observation period. Constant efficiency is an important factor when studying interannual trends as well as extreme events, such as the eruption of the Tonga volcano.

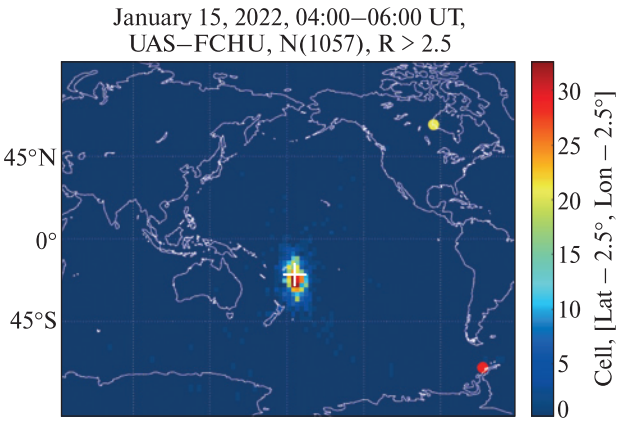

Figure 9. Distribution of intense lightning strikes geolocated from UAS (red circle) and FCHU (yellow circle) sites on January 15, 2022 (04:00–06:00 UT). The location of the Tonga volcano is shown by the white cross. The number of lightning strokes in the cells 2.5°–2.5° is presented in false colors

• Observations at UAS and CARISMA are financed within the framework of existing scientific projects and do not require additional funding.

The main promising scientific and practical problems for the analyzed system include the following:

• Lightning activity, estimated by variations in the integral level of Schumann resonances, is a proxy for changes in global temperature. Since the techniques described above make it possible to evaluate activities separately for each of the worldwide thunderstorm centers on timescales from minutes to tens of years, there is a potential opportunity to monitor both short-term climate trends (Bozóki et al., 2023) and explore the phenomenon of global warming (Williams, 2020). From our point of view, this is the principal scientific and practically significant task for the described ELF network.

• Climate warming and the increase in lightning activity most intensively occur in high latitudes (Chen et al., 2021; Holzwort et al., 2021). Monitoring integral thunderstorm activity and intense lightning makes it possible to study these trends, compare them with other regions, and forecast when these effects can begin to affect people and technology in polar areas.

This is important because, in the polar regions, thunderstorms were previously generally not observed at all and, therefore, lightning protection devices were not used. Thus, critical infrastructure objects must now be equipped with these devices, which is tricky logistically and requires significant funding. Therefore, the prediction of safe deadlines for such an upgrade is very relevant.

• The presence of two (or more) far-separated points allows simultaneous monitoring of integral thunderstorm activity and super-powerful lightning (i.e., precisely those phenomena that pose the greatest danger to humans and technology). Thus, it is possible to compare integral activity and the distribution of super-powerful lightning in space and time. To our knowledge, such observations have not been systematically carried out before.

• Analysis of SR data measured at high latitudes makes it possible to study the effect of Schumann resonance intensity modulation discovered at Vernadsky (Nickolaenko et al., 2015; Koloskov et al., 2020a; Bozóki et al., 2021) because of precipitation of charged particles in auroral regions. This will allow: a) using Schumann resonance data as a proxy for precipitation intensity which is an essential practical task for diagnostics of auroral activities posing risks to humans and technological systems; b) calculating the influence of space weather phenomena on the observed Schumann resonance intensity using external data on precipitation to reconstruct the initial (not distorted by the medium) activities of thunderstorm centers. This is an essential practical task for tracking global temperature trends.

5 Conclusions

The analysis of ELF records obtained by the CARISMA/UAS magnetometer network, along with the previously validated data processing techniques at UAS, proves to be effective in monitoring both overall (through Schumann spectra processing) and intense lightning activity (by analyzing transients and geolocating strikes). This comprehensive observation approach allows for the examination of integral and intense lightning activity in both spatial and temporal dimensions, with characteristic timescales spanning from minutes to several decades. Such a systematic analysis has not been conducted previously.

During the eruption of the Hunga Tonga-Hunga Ha'apai volcano on January 15, 2022, the processing of ELF data demonstrates distinct indications of heightened lightning activity in the vicinity of the epicenter, evident in both Schumann spectra and transients. Notably, the number of ordinary and intense lightning strikes above the epicenter substantially surpassed the combined count of lightning occurrences in all other regions of the Earth at the peak of the eruption. This observation presents an opportunity to investigate the influence of volcanic activity on climate dynamics and refine the point source model for the propagation of resonant ELF signals within the Earth-ionosphere cavity.

The primary and significant scientific task of monitoring the ELF network involves analyzing global thunderstorm activity as a proxy for assessing temperature variations on the planet over timescales ranging from several days to tens of years. The objective is to identify and predict global climate changes. Additionally, a crucial practical task is to study and anticipate the escalating trend of lightning activity in high latitudes, where it has been increasing faster than in middle and low latitudes in recent years. Analyzing Schumann signals at high latitudes can aid in understanding variations associated with the modulation of the ionospheric boundary properties by space weather phenomena. This analysis enables the diagnosing and predicting disturbances in the auroral plasma, posing potential risks to human activities and technological systems.

Overall, the systematic study of ELF data, together with the analysis of lightning activity, presents an opportunity for valuable insights into global climate dynamics and space weather impacts, contributing to improved risk assessment and prediction capabilities.

Data availability. CARISMA ELF data can be requested from https://www.carisma.ca/carisma-data-repository. Vernadsky station ELF data can be requested from the State Institution National Antarctic Scientific Center: uac@uac.gov.ua

Author contributions. The idea, data processing, and illustration preparation: O.K. Data acquisition and preparation: O.K. Interpretation of the results: O.K., P.T.J., and Y.Y. Writing: O.K., P.T.J., and Y.Y. Manuscript review and editing: O.K., P.T.J., and Y.Y. All authors have read and agree to publish the current version of the manuscript.

Acknowledgments. The authors thank I. R. Mann, D. K. Milling and the rest of the CARISMA team for the data provided. CARISMA is operated by the University of Alberta, funded by the Canadian Space Agency. We are truly thankful to the State Institution National Antarctic Scientific Center and its staff members for providing the support including funding and logistics for all the Antarctic operations involved and to the winterers of the Ukrainian Antarctic Expeditions for care and maintenance of the ELF facilities. We would like to express special gratitude to the Armed Forces of Ukraine for their heroic struggle and courage that allowed Ukrainian scientists to continue their research activities.

Funding. The State Special-Purpose Research Program in Antarctica for 2011–2023 project #0121U108635 funded by the Ministry of Education and Science of Ukraine and partially supported by EOARD-STCU Partner Project P-775 (EOARD 22IOE019) and "Heliomax-2023" Project funded by the State Institution National Antarctic Scientific Center.

Conflict of Interest. The authors declare no conflict of interests.

References

Astafyeva, E., Maletckii, B., Mikesell, T. D., Munaibari, E., Ravanelli, M., Coisson, P., Manta, F., & Rolland, L. (2022). The 15 January 2022 Hunga Tonga eruption history as inferred from ionospheric observations. *Geophysical Research Letters*, *49*(10), e2022GL098827. https://doi.org/10.1029/2022GL098827

Balser, M., & Wagner, C. A. (1960). Observation of Earth-ionosphere cavity resonances. *Nature*, *188*, 638–641. https://doi.org/10.1038/188638a0

Bezrodny, V., Budanov, O., Koloskov, A. V., Hayakawa, M., Sinitsin, V., Yampolski, Y., & Korepanov, V. (2007). The ELF band as a possible spectral window for seismo-ionospheric diagnostics. *Sun and Geosphere*, *2*(2), 88–95.

Bliokh, P. V., Nikolaenko, A. P., & Filippov, Yu. F. (1980). *Schumann resonances in the Earth-ionosphere cavity* (D. LIanwyn-Jones, Ed.). Peter Peregrinus Ltd on behalf of the Institution of Electrical Engineers.

Bór, J., Bozóki, T., Sátori, G., Williams, E., Behnke, S. A., Rycroft, M. J., Buzás, A., Silva, H. G., Kubicki, M., Said, R., Vagasky, C., Steinbach, P., Szabóné André, K., & Atkinson, M. (2023). Responses of the AC/DC global electric circuit to volcanic electrical activity in the Hunga Tonga-Hunga Ha'apai eruption on 15 January 2022. *Journal of Geophysical Research: Atmospheres*, *128* (8), e2022JD038238. https://doi.org/10.1029/2022JD038238

Born, M., & Wolf, E. (1959). *Principles of optics*. Pergamon Press Ltd.

Bozóki, T., Sátori, G., Williams, E., Mironova, I., Steinbach, P., Bland, E. C., Koloskov, A., Yampolski, Yu. M., Budanov, O. V., Neska, M., Sinha, A. K., Rawat, R., Sato, M., Beggan, C. D., Toledo-Redondo, S., Liu,Y., & Boldi, R. (2021). Solar cycle-modulated deformation of the Earth–ionosphere cavity. *Frontiers in Earth Science*, *9*. https://doi.org/10.3389/feart.2021.689127

Bozóki, T., Sátori, G., Williams, E., Guha, A., Liu, Y., Steinbach, P., Leal, A., Herein, M., Atkinson, M., Beggan, C. D., DiGangi, E., Koloskov, A., Kulak, A., LaPierre, J., Milling, D. K., Mlynarczyk, J., Neska, A., Potapov, A., Raita, T., Rawat, R., Said, R., Sinha, A. K., & Yampolski, Y. (2023). Day-to-day quantification of changes in global lightning activity based on Schumann resonances. *Journal of Geophysical Research: Atmospheres*, *128*, e2023JD038557. https://doi.org/10.1029/2023JD038557

Chen, Y., Romps, D. M., Seeley, J. T., Veraverbeke, S., Riley, W. J., Mekonnen, Z. A., & Randerson, J. T. (2021). Future increases in Arctic lightning and fire risk for permafrost carbon. *Nature Climate Change*, *11*, 404–410. https://doi.org/10.1038/s41558-021-01011-y

Cherry, N. (2002). Schumann Resonances, a plausible biophysical mechanism for the human health effects of Solar. *Natural Hazards, 26,* 279–331. https://doi.org/10.1023/A:1015637127504

Christian, H. J., Blakeslee, R. J., Boccippio, D. J., Boeck, W. L., Buechler, D. E., Driscoll, K. T., Goodman, S. J., Hall, J. M., Koshak, W. J., Mach, D. M., & Stewart, M. F. (2003). Global frequency and distribution of lightning as observed from space by the Optical Transient Detector. *Journal of Geophysical Research: Atmospheres*, *108*(D1), 4005. https://doi.org/10.1029/2002JD002347

Füllekrug, M., & Constable, S. (2000). Global triangulation of intense lightning discharges. *Geophysical Research Letters, 27*(3), 333–336. https://doi.org/10.1029/1999GL003684

Füllekrug, M., & Fraser-Smith, A. C. (1997). Global lightning and climate variability inferred from ELF magnetic field observations. *Geophysical Research Letters, 24*(19), 2411–2414. https://doi.org/10.1029/97GL02358

Gurnett, D. A., & Bhattacharjee, A. (2017). *Introduction to plasma physics: with space, laboratory and astrophysical applications* (2nd ed.). Cambridge University Press. https://doi.org/10.1017/9781139226059

Hobara, Y., Harada, T., Ohta, K., Sekiguchi, M., & Hayakawa, M. (2011). A study on global temperature and thunderstorm activity by using the data of Schumann resonance observed at Nakatsugawa, Japan. *Journal of Atmospheric Electricity, 31*(2), 111–119. https://doi.org/10.1541/jae.31

Holzworth, R. H., Brundell, J. B., McCarthy, M. P., Jacobson, A. R., Rodger, C. J., & Anderson, T. S. (2021). Lightning in the Arctic. *Geophysical Research Letters, 48*(7), e2020GL091366. https://doi.org/10.1029/2020GL091366

Huang, Y. S., Tang, I., Chin, W. C., Jang, L. S., Lee, L. C., Lin, C., Yang, C. P., & Cho, S. L. (2022). The subjective and objective improvement of non-invasive treatment of Schumann resonance in insomnia — a randomized and double-blinded study. *Nature and Science of Sleep, 14*, 1113–1124. https://doi.org/10.2147/NSS.S346941

Koloskov, A. V., Bezrodny, V. G., Budanov, O. V., Paznukhov, V. E., & Yampolski, Yu. M. (2005). Polarization monitoring of the Schumann resonances in the Antarctic and reconstruction of the world thunderstorm activity characteristics. *Radio Physics and Radio Astronomy, 10*(1), 11–29. (in Russian)

Koloskov, A. V., Baru, N. A., Budanov, O. V., Bezrodny, V. G., Gavriluk, B. Yu., Paznukhov, A. V., & Yampolski, Yu. M. (2013). Diagnostic of the global lightning activity based on the data of long-term monitoring of the Schumann resonance signals at UAS Akademician Vernadsky. *Ukrainian Antarctic Journal,* 12, 170–176. (in Russian)

Koloskov, A. V., Nickolaenko, A. P., Yampolsky, Yu. M., Hall, C., & Budanov, O. V. (2020a). Variations of global thunderstorm activity derived from the long-term Schumann resonance monitoring in the Antarctic and in the Arctic. *Journal of Atmospheric and Solar-Terrestrial Physics, 201*, 105231. https://doi.org/10.1016/j.jastp.2020.105231

Koloskov, A., Shvets, A., Nickolaenko, A., Yampolski, Yu., Budanov, O., & Shvets, A. (2020b). Studying the powerful lightning discharges from the Antarctic and the Arctic stations using synchronous ELF and VLF data. In *URSI GASS 2020, Rome, Italy, 29 August – 5 September 2020.* http://www.ursi.org/proceedings/procGA20/papers/KoloskovetalELFVLFExtendedAbstract.pdf

Koloskov, O. V., Nickolaenko, A. P., Yampolski, Y. M., & Budanov, O. V. (2022). Electromagnetic seasons in Schumann resonance records. *Journal of Geophysical Research: Atmospheres, 127*(17), e2022JD036582. https://doi.org/10.1029/2022JD036582

Mann, I. R., Milling, D. K., Rae, I. J., Ozeke, L. G., Kale, A., Kale, Z. C., Murphy, K. R., Parent, A., Usanova, M., Pahud, D. M., Lee, E.-A., Amalraj, V., Wallis, D. D., Angelopoulos, V., Glassmeier, K.-H., Russell, C. T., Auster, H.-U., & Singer, H. J. (2008). The upgraded CARISMA magnetometer array in the THEMIS era. *Space Science Reviews, 141*, 413–451, https://doi.org/10.1007/s11214-008-9457-6.

Mezentsev, A., Nickolaenko, A. P., Shvets, A. V., Galuk, Yu. P., Schekotov, A. Yu., Hayakawa, M., Romero, R., Izutsu, J., & Kudintseva, I. G. (2023). Observational and model impact of Tonga volcano eruption on Schumann resonance. *Journal of Geophysical Research: Atmospheres, 128*(7), e2022JD037841. https://doi.org/10.1029/2022JD037841

Nickolaenko, A. P., & Hayakawa, M. (2002). *Resonances in the Earth-ionosphere cavity*. Kluwer Academic Publishers.

Nickolaenko, A. P., & Hayakawa, M. (2014). *Schumann resonance for tyros (Essentials of global electromagnetic resonance in the Earth–ionosphere cavity)*. Springer Tokyo. https://doi.org/10.1007/978-4-431-54358-9

Nickolaenko, A. P., Koloskov, A. V., Hayakawa, M., Yampolski, Yu. M., Budanov, O. V., & Korepanov, V. E. (2015). 11-year solar cycle in Schumann resonance data as observed in Antarctica. *Sun and Geosphere, 10*(1), 39–49.

Nickolaenko, A., Schekotov, A. Yu., Hayakawa, M., Romero, R., & Izutsu, J. (2022). Electromagnetic manifestations of Tonga eruption in Schumann resonance band. *Journal of Atmospheric and Solar-Terrestrial Physics, 237*, 105897.

Ondraskova, A., Sevcík, S., & Kostecký, P. (2009). A significant decrease of the fundamental Schumann resonance frequency during the solar cycle minimum of 2008-9 as observed at Modra Observatory. *Contributions to Geophysics & Geodesy, 39*(4), 345–354. https://doi.org/10.2478/v10126-009-0013-5

Paznukhov, A. V., Yampolski, Y. M., Koloskov, A. V., Hall, C., Paznukhov, V. E., & Budanov, O. V. (2019). Correlation between air temperature and thunderstorm activity in Africa according to the ELF measurements in Antarctica, Arctica and Ukraine. *Radio Physics and Radio Astronomy, 24*(3), 195–205. https://doi.org/10.15407/rpra24.03.195 (in Russian)

Paznukhov, A. V., Yampolski, Y. M., & Koloskov, A. V. (2020). Correlation between air temperature and thunderstorm activity in South America according to the ELF measurements in Antarctica. *Radio Physics and Radio Astronomy, 25*(3), 211–217. https://doi.org/10.15407/rpra25.03.211 (in Ukrainian)

Peterson, M., Mach, D., & Buechler, D. (2021). A global LIS/OTD climatology of lightning flash extent density. *Journal of Geophysical Research: Atmospheres*, *126*(8), e2020JD033885. https://doi.org/10.1029/2020JD033885

Pizzuti, A., Bennett, A., & Füllekrug, M. (2022). Long-term observations of Schumann resonances at Portishead (UK). *Atmosphere, 13*(1), 38. https://doi.org/10.3390/atmos13010038

Plotnik, T., Price, C., Saha, J., & Guha, A. (2021). Transport of water vapor from tropical cyclones to the upper troposphere. *Atmosphere*, *12*(11), 1506. https://doi.org/10.3390/atmos12111506

Price, C. (2000). Evidence for a link between global lightning activity and upper tropospheric water vapour. *Nature*, *406*, 290–293. https://doi.org/10.1038/35018543

Price, C., & Rind, D. (1990). The effect of global warming on lightning frequencies. In *Conference on Severe Local Storms* (pp. 748–751). AMS.

Price, C., Penner, J., & Prather, M. (1997). NO_x from lightning: 1. Global distribution based on lightning physics. *Journal of Geophysical Research: Atmospheres*, *102*(D5), 5929–5941. https://doi.org/10.1029/96JD03504

Price, C., Williams, E., Elhalel, G., & Sentman, D. (2021). Natural ELF fields in the atmosphere and in living organisms. *International Journal of Biometeorology, 65*(1), 85–92. https://doi.org/10.1007/s00484-020-01864-6

Roldugin, V. C., Maltsev, Y. P., Vasiljev, A. N., Shvets, A. V., & Nikolaenko, A. P. (2003). Changes of Schumann resonance parameters during the solar proton event of 14 July 2000. *Journal of Geophysical Research: Space Physics, 108*(A3). https://doi.org/10.1029/2002JA009495

Rycroft, M. J., Israelsson, S., & Price, C. (2000). The global atmospheric electric circuit, solar activity and climate change. *Journal of Atmospheric and Solar-Terrestrial Physics, 62*(17–18), 1563–1576. https://doi.org/10.1016/S1364-6826(00)00112-7

Sátori, G. (1996). Monitoring Schumann resonances – 11. Daily and seasonal frequency variations. *Journal of Atmospheric and Terrestrial Physics, 58*(13), 1483–1488. https://doi.org/10.1016/0021-9169(95)00146-8

Sátori, G., Szendrői, J., & Verő, J. (1996). Monitoring Schumann resonances – I. Methodology. *Journal of Atmospheric and Terrestrial Physics*, *58*(13), 1475–1481. https://doi.org/10.1016/0021-9169(95)00145-X

Sátori, G., Williams, E., & Mushtak, V. (2005). Response of the Earth–ionosphere cavity resonator to the 11-year solar cycle in X-radiation. *Journal of Atmospheric and Solar-Terrestrial Physics, 67*(6), 553–562. https://doi.org/10.1016/j.jastp.2004.12.006

Sátori, G., Williams, E., Price, C., Boldi, R., Koloskov, A., Yampolski, Y., Guha, A., & Barta, V. (2016). Effects of Energetic Solar Emissions on the Earth-Ionosphere Cavity of Schumann Resonances. *Surveys in Geophysics, 37*, 757–789. https://doi.org/10.1007/s10712-016-9369-z

Schlegel, K., & Füllekrug, M. (1999). Schumann resonance parameter changes during high-energy particle precipitation. *Journal of Geophysical Research: Space Physics, 104*(A5), 10,111–10,118. https://doi.org/10.1029/1999JA900056

Schumann, W. O. (1952). Über die strahlungslosen Eigenschwingungen einer leitenden Kugel, die von einer Luftschicht und einer Ionosphärenhülleumgebenist. *Zeitschrift für Naturforschung A, 7*(2), 149–154. https://doi.org/10.1515/zna-1952-0202

Sekiguchi, M., Hayakawa, M., Nickolaenko, A. P., & Hobara, Y. (2006). Evidence on a link between the intensity of Schumann resonance and global surface temperature. *Annales Geophysicae, 24*(7), 1809–1817. https://doi.org/10.5194/angeo-24-1809-2006

Sentman, D. D., & Fraser, B. J. (1991). Simultaneous observations of Schumann resonances in California and Australia: evidence for intensity modulation by the local height of the D-region. *Journal of Geophysical Research: Space Physics, 96*(A9), 15973–15984. https://doi.org/10.1029/91JA01085

Shvets, A. V., Ivanov, V. K., & Varavin, A. V. (2003). A mobile multichannel system for the automatic low-frequency signal acquisition and analysis in the presence of high-power power-main noises. *Instruments and Experimental Techniques, 46*(3), 351–356. https://doi.org/10.1023/A:1024462304875

Shvets, A. V., Nickolaenko, A. P., Koloskov, A. V., Yampolsky, Yu. M., Budanov, O. V., & Shvets, A. A. (2022). Day after day variations of arrival angles and polarisation parameters of Q bursts recorded at Antarctic station "Akademik Vernadsky". *Journal of Atmospheric and Solar–Terrestrial Physics, 229*, 105811. https://doi.org/10.1016/j.jastp.2021.105811

Surkov, V., & Hayakawa, M. (2014). *Ultra and extremely low frequency electromagnetic fields.* Springer Tokyo. https://doi.org/10.1007/978-4-431-54367-1

Timofejeva, I., McCraty, R., Atkinson, M., Alabdulgader, A. A., Vainoras, A., Landauskas, M., Šiaučiūnaitė, V., & Ragulskis, M. (2021). Global study of human heart rhythm synchronization with the Earth's time varying magnetic field. *Applied Sciences, 11*, 2935. https://doi.org/10.3390/app11072935

Vagasky, C., & Said, R. (2022). Did the eruption of Hunga Tonga-Hunga Ha'apai produce the greatest concentration of lightning ever detected? In *AGU Fall Meeting, Chicago IL, 12–16 December, 2022. Science leads the future*. https://agu.confex.com/agu/fm22/meetingapp.cgi/Paper/1157649

Williams, E. R. (1992). The Schumann resonance: A global tropical thermometer. *Science, 256*(5060), 1184–1187. https://doi.org/10.1126/science.256.5060.1184

Williams, E. R. (2005). Lightning and climate: A review. *Atmospheric Research, 76*(1–4), 272–287. https://doi.org/10.1016/j.atmosres.2004.11.014

Williams, E. R. (2020). Lightning and Climate Change. In A. Piantini (Ed.), *Lightning Interaction with Power Systems* (Vol. 1, pp. 1–45). The Institution of Engineering and Technology.

Williams, E., Guha, A., Boldi, R., Sátori, G., Koloskov, A., & Yampolski, Y. (2014). Global circuit response to the 11-year solar cycle: changes in source or in medium? In *XV International conference on atmospheric electricity, 15–20 June 2014, Norman, Oklahoma*. https://www.nssl.noaa.gov/users/mansell/icae2014/preprints/Williams_299.pdf

Williams, E., Guha, A., Boldi, R., Christian, H., & Buechler, D. (2019). Global lightning activity and the hiatus in global warming. *Journal of Atmospheric and Solar-Terrestrial Physics, 189*, 27–34. https://doi.org/10.1016/j.jastp.2019.03.011

Williams, E., Montanya, J., Saha, J., & Guha, A. (2023). Lightning and Climate Change. In V. Cooray, F. Rachidi, & M. Rubinstein (Eds.), *Lightning Electromagnetics* (2nd ed., Vol. 2, pp. 569–626). Institute of Engineering and Technology.

Received: 25 May 2023
Accepted: 22 July 2023

О. Колосков[1, 2, 3], П. Т. Джаячандран[1], Ю. Ямпольський[3]

[1] Університет Нью-Брансвік, м. Фредеріктон, Нью-Брансвік, E3B5A3, Канада
[2] Державна установа Національний антарктичний науковий центр МОН України, м. Київ, 01601, Україна
[3] Радіоастрономічний інститут НАН України, м. Харків, 61002, Україна

*** Автор для кореспонденції:** alex.koloskov@und.ca

Ефективність моніторингу Шуманівського резонансу мережею CARISMA – станція «Академік Вернадський»

Реферат. Головною метою цього дослідження є оцінка ефективності мережі низькочастотних індукційних магнітометрів, утворених CARISMA (Канадський Масив Досліджень Магнітної Активності Реального Часу) та станцією «Академік Вернадський» (65.25°S 64.25°W, далі – Вернадський), як системи планетарного моніторингу грозової активності зі спостережними пунктами, розташованими в Арктичному та Антарктичному регіонах відповідно. Для досягнення цієї мети були оброблені та проаналізовані добові записи надзвичайно низькочастотних сигналів (ННЧ) з Вернадського та Форт Черчілл (FCHU, 58.76°S 94.08°W), зібрані в січні 2022 року. Для CARISMA були використані дані з пункту FCHU через краще співвідношення сигнал-шум. Горизонтальні магнітні компоненти сигналів Шумана, отримані на Вернадському та FCHU, пройшли спектральну та поляризаційну обробку. Виявлено та далі здійснено геолокацію ННЧ транзієнтів, для періодів регулярної (спокійної) грозової активності і несподіваного локального посилення блискавкової активності біля вулкану Хунга-Тонга-Хунга-Хаапай під час його виверження 15 січня 2022 року. Під час спокійних періодів в результаті обробки ННЧ сигналів отриманих на мережі CARISMA-Вернадський отримано характеристики інтегральної блискавкової активності, які добре узгоджуються з літературними даними та результатами попередніх досліджень на станції «Академік Вернадський». З іншого боку, аналіз спектрів Шумана та ННЧ транзієнтів під час виверження вулкану Хунга-Тонга-Хунга-Хаапай підтвердив, що більшість гроз була сконцентрована в невеликій області навколо епіцентру, а це підтверджує модель точкового джерела для цього світового центру блискавок. Стаття демонструє, що мережа магнітометрів CARISMA-Вернадський підходить для створення глобальної системи моніторингу блискавкової активності та точної геолокації потужних блискавок. Така система може бути використана для оцінки та вивчення глобальних температурних трендів, моніторингу зростання блискавкової активності у високих широтах, а також виявлення явищ наземних, атмосферних та геокосмічних катастроф.

Ключові слова: глобальні зміни клімату, космічна погода, мережа виявлення блискавок, надзвичайно низька частота, транзієнтні події